

THE MOLONGLO GALACTIC PLANE SURVEY.

I. OVERVIEW AND IMAGES

A. J. Green, L. E. Cram, M. I. Large

and

Taisheng Ye

School of Physics, University of Sydney 2006, Australia

A.Green@physics.usyd.edu.au, L.Cram@physics.usyd.edu.au,

M.Large@physics.usyd.edu.au, tye@atnf.csiro.au

ABSTRACT

The first epoch Molonglo Galactic Plane Survey (MGPS1) is a radio continuum survey made using the Molonglo Observatory Synthesis Telescope (MOST) at 843 MHz with a resolution of $43'' \times 43''$ cosec $|\delta|$. The region surveyed is $245^\circ \leq l \leq 355^\circ, |b| \leq 1.5^\circ$. The thirteen $9^\circ \times 3^\circ$ mosaic images presented here are the superposition of over 450 complete synthesis observations, each taking 12 h and covering a field of $70' \times 70'$ cosec $|\delta|$. The root-mean-square sensitivity over much of the mosaiced survey is 1–2 mJy beam $^{-1}$ (1σ), and the positional accuracy is $\approx 1'' \times 1''$ cosec $|\delta|$ for sources brighter than 20 mJy. The dynamic range is no better than 250:1, and this also constrains the sensitivity in some parts of the images. The survey area of 330 deg^2 contains well over 1.2×10^4 unresolved or barely resolved objects, almost all of which are extra-galactic sources lying in the Zone of Avoidance. In addition a significant fraction of this area is covered by extended, diffuse emission associated with thermal complexes, discrete H II regions, supernova remnants, and other structures in the Galactic interstellar medium.

Subject headings: Galaxy: structure — radio continuum: ISM — surveys

1. Introduction

The area of sky close to the Galactic equator produces radio emission on a wide range of angular scales. To unravel the nature of the complex radio structures seen in the Plane, a high resolution survey is essential. The Molonglo Observatory Synthesis Telescope (MOST)

is well suited to this task, producing large images ($70' \times 70' \operatorname{cosec} |\delta|$) with sub-arcminute angular resolution and a sensitivity (1σ) of 1–2 mJy beam $^{-1}$. Accordingly, the southern Galactic Plane has been surveyed with the MOST in the radio continuum at 843 MHz, covering the area $245^\circ \leq l \leq 355^\circ$, $|b| \leq 1.5^\circ$, with a resolution of $43'' \times 43'' \operatorname{cosec} |\delta|$. A report on the early progress of the survey was published by Whiteoak et al. (1989). The final data set is a compilation of more than 450 overlapping fields which have been assembled as a series of $3^\circ \times 3^\circ$ mosaics under the title of the First Epoch Molonglo Galactic Plane Survey (MGPS1). The mosaics are presented here in Galactic co-ordinates, in panels covering $9^\circ \times 3^\circ$ for ease of viewing.

No previous large-scale radio survey of the southern Galaxy has superior angular resolution or sensitivity. MGPS1 extends and complements other radio surveys such as the 2.3 GHz Parkes survey (Duncan et al. 1995) with $10'$ resolution, the HI galaxy search along the Galactic Plane with a resolution of $15'$ (Staveley-Smith et al. 1998), several Parkes surveys at 5 GHz (Griffith, Wright et al. 1993; Haynes, Caswell & Simons 1978; Goss & Shaver 1970), and the 408 MHz Mills Cross surveys (Shaver & Goss 1970; Green 1974). The 1.4 GHz VLA¹ Sky Survey (NVSS) of Condon et al. (1998) has similar resolution and greater sensitivity than the MGPS1 survey, but unfortunately the overlap region is only about 20° of longitude at either end. The northern hemisphere Westerbork Galactic Plane Survey at 327 MHz (Taylor et al. 1996) has similar resolution and sensitivity to MGPS1 and many of the outcomes from that survey will have a counterpart in the present work.

This paper presents the strategies used to produce the survey in Section 2, an outline of the reduction procedures including an assessment of the quality and limitations of the data in Section 3, and the results from the survey in Section 4. MOST studies of the Galactic Centre (Gray 1994a,b,c,d) and the Vela supernova remnant (Bock, Turtle & Green 1998) should be regarded as extensions of this survey.

2. Observations

The MOST is an Earth-rotation synthesis radio telescope with the technical parameters listed in Table 1. For the survey reported here, all observations were made in a time-shared mode for which the field of view is $70' \times 70' \operatorname{cosec} |\delta|$. As explained by Mills (1981) and Robertson (1991), the MOST is distinguished from other Earth-rotation synthesis telescopes by two principal differences.

¹the Very Large Array of the National Radio Astronomy Observatory

Firstly, the MOST is an east-west cylindrical paraboloid reflector which illuminates a line feed comprising nearly nine thousand ring elements. It tracks a point in the sky by mechanically steering the *tilt* of the reflector about its long axis, and electronically and mechanically steering the *meridian distance* of the cone beams formed by the feed line. Figure 1 illustrates the tilt and meridian distance (*MD*) co-ordinates which form a natural system for the MOST.

The combination of (slow) mechanical and (fast) electronic steering of the cone beams, taken together with the regular spacing of the sub-structures which comprise the feed line, leads to grating responses lying 1.15° sec (*MD*) away from the central response. The amplitude of these is small near the centre of the field but, if uncorrected, rises to about 20% of the central response at the edge of the field. Deconvolution of these responses has proven to be difficult, but modifications (Amy & Large 1989) undertaken during the course of the survey significantly reduced their amplitude. In addition to inducing grating responses, the long, cylindrical form of the MOST also forms an instantaneous primary beam which is not azimuthally symmetric. This implies that different parts of a synthesised image are subject to different attenuation, resulting from the integrated effect of the time-varying instantaneous primary beam. We call this attenuation the ‘synthesised primary beam.’ No difficulties are encountered in dealing with its effect on the images.

The second distinguishing characteristic of the MOST is that it forms fan beam responses in real time and records these directly, thus bypassing the need to record complex visibilities. This process greatly reduces the required computing power, but entails vector averaging over all redundant baselines. Such averaging removes the possibility of antenna-based self calibration. The consequences of these differences are discussed below.

With a field of view of $70' \times 70'$ cosec $|\delta|$, the MOST is well suited to imaging large areas of the sky. Nevertheless, a complete survey of the southern Galactic plane has necessitated a number of compromises whose impact on the survey are described below.

2.1. Observing Strategies

Complete synthesis of MOST images requires full coverage of hour angles, h , satisfying $-6^h \leq h \leq +6^h$. This is done by tracking the field centre for 12 h, sampling the fan-beam responses every 24 s. Owing to (intended) mechanical limitations in the MOST, complete synthesis is possible only for declinations south of approximately -30° . The survey has thus been restricted to $245^\circ \leq l \leq 355^\circ$. Gray (1994a,b,c,d) has surveyed a $10^\circ \times 5^\circ$ ($l \times b$) field at the Galactic centre which should be regarded as the northern extension of the survey

presented here.

Being an east-west array, the MOST forms an elliptical synthesised interferometer beam that is elongated by a factor of $\text{cosec } |\delta|$ in declination relative to right ascension. The field of view within the synthesised primary beam has a similar aspect ratio. When this fact is combined with the arc-like projection of the Galactic plane onto the southern sky, it implies that a rather complex grid of standard field centres is needed to cover the survey area efficiently. In addition, to minimize the challenges of dealing with the grating responses described above it was desirable to allow for considerable overlap of fields. A standard survey grid was adopted in which adjacent fields overlap to within $\sim 10'$ of the field centres. Many additional observations were made with non-standard field centres, to further reduce the impact of grating responses and other artifacts produced in the observations positioned on the standard grid. The surveyed area and the coverage is illustrated in Figure 2.

Preferentially, MOST synthesis observations are made at night with the field centre transiting near midnight. This minimises the effects of solar radiation at radio frequencies and reduces exposure to artificial interference. Consequently, most observations were made each year between February and June. The complete log of the 455 observations used in the survey is listed in Table 2, which gives the Galactic name of each field observed, the RA and Dec. at epoch J2000 of the pointing centre, the date of observation, and a flag (N) if the field was not part of the standard grid. This Table will allow users of the survey to identify component fields containing selected sources, and also facilitate searches for variability of sources detected at different times in this survey, or in any future work. In cases when pointing centres were repeated, multiple dates are given only for data actually used in the final survey.

2.2. Primary Calibration

The primary calibration of images in the survey rests on observations of a sample of strong, compact sources made immediately before and after each 12 hour synthesis. These short fan-beam observations are known as ‘scans.’ The 843 MHz flux densities and positions of the calibration sources have been compiled by Hunstead (1991) and updated (cataloguing known source variability) by Campbell-Wilson & Hunstead (1994). The absolute flux density scale is believed to be accurate to $\pm 5\%$, and the positions are tied to the southern VLBI frame to an uncertainty of about ± 0.5 arcsec. The output of a scan observation of a calibration source is an estimate of the gain of the telescope (counts Jy^{-1}) and the pointing offset in meridian distance (arcsec). To reduce the effects of confusion, intrinsic variability and scintillation on the calibration parameters, up to 8 sources are

observed before and another 8 after each synthesis observation. The gain and pointing offsets are determined for each of these sources and a median fit to the entire set is used to calibrate the corresponding image.

The large amount of overlap in the component fields of the survey allows refinement of the calibration factors after the entire data set has been analyzed. To do this, the flux densities and positions of strong, unresolved sources detected in each image were assembled into a data base, which collated the multiple measurements that exist for many of the sources. Median filtering of these repeated measurements provided an additional calibration correction for each image, which could be applied either by re-imaging or during the assembly of the mosaics (Section 3.2).

The variation in the mean of the daily scan calibration factors is about 10% for the gain, and $2.0''$ for the meridian distance offset (which leads to a positional uncertainty of about $2.5''$ in the final image). The use of overlapping fields reduced these to about 5% for the final flux density scale, and to about $1'' \times 1'' \csc |\delta|$ in position, for sources stronger than 20 mJy. As we note below, the complexity and high brightness of much Galactic emission ensures that for a significant fraction of the survey, the image quality is not determined by calibration uncertainties.

3. Data Analysis

The formation of the final data product of the survey has involved many time-consuming and often complex computations, mainly to deal with artefacts. While the details of these processes are not necessarily of general interest, it is important that users of the survey appreciate all of the significant consequences for subsequent interpretation of the images. Hence, we provide here a brief but fairly complete account of the reduction procedures.

3.1. Editing & Auxiliary Calibration

MOST data are corrupted on occasion by artificial radio sources (principally mobile telephones) and by electromagnetic radiation associated with lightning and the Sun. Typically, only 0 – 10 samples (each of 24 solar seconds duration) are affected by artificial interference or lightning in any 12 (sidereal) hour data set of 1796 samples, but in view of the large amplitude of some of the interference it must be removed prior to image formation. The corrupted samples are identified during automated or visual inspection of the raw data and then deleted. Solar interference has a different character, being manifest as low-level,

large scale bands aligned in directions corresponding to the hour angles at which the Sun lies in one of the MOST's sidelobes. Despite the complexity of the telescope response to the Sun, solar interference can be satisfactorily removed by carefully adjusting the baselevel of the image using Fourier techniques.

Most sample deletions can be compensated for by ensuring that the shape and amplitude of the corresponding deconvolution beam correctly reflects their existence. Nevertheless, in images where there is a very strong source located just outside the field in question, it is not possible to CLEAN the sidelobes of this source completely. A radial artefact at the hour angle of any deleted sample will be produced. There are only a few such artefacts remaining in the survey, most of them having been removed interactively by using the relevant overlapped images which are free from interference at the hour angles in question.

In addition to the primary calibration of the daily flux density scale described above, auxiliary calibrations must be made to correct for (1) environmental variations, (2) attenuation due to the primary beam, and (3) variation of the telescope gain as a field is tracked in meridian distance.

The main environmental correction arises from the thermal sensitivity of several components in the receiver chain exposed to the atmosphere. The temperature sensitivity of the throughput of the entire system is determined from time to time by tests which show that the calibration factor is well-described by a stable function of temperature. To evaluate this function, the ambient temperature is measured and recorded with each data sample. The uncertainty in the flux density scale due to this calibration is approximately $\pm 1\%$. The gain of the telescope is sometimes reduced anomalously following periods of rain, due to attenuation in the local oscillator trough line. The few observations badly compromised by wet weather have been rejected and the field subsequently repeated.

Because the MOST is a cylindrical paraboloid, the projection of the primary beam in the image plane varies with the hour angle of the field centre. This variation is readily modelled on the basis of telescope calibrations performed prior to the survey, and can be easily removed in the imaging process. Even at the declination extremes of the most northerly fields in the survey, where the effects of the primary beam attenuation are largest, the correction is no more than a factor of 1.2, with an uncertainty no larger than 10% of this value. The correction is much smaller over most of the surveyed area.

The variation of telescope gain with meridian distance (called the ‘meridian distance gain curve’) consist of two parts. The first is a monotonic decline towards large meridian distances due to the foreshortening of the collecting area of the horizontal paraboloid. The

second is a modulation of order $\pm 20\%$ on an angular scale of about 10° , due to constructive and destructive interference between rays that are directly reflected, and those scattered from the feed line and its supports. The meridian distance gain curve of the telescope is invariant and calibrated with an uncertainty of about 2%. A correction for the modulation is readily made in the imaging process.

3.2. Image Formation

A flow chart of the procedure used to produce the final images is shown in Figure 3. It involves two major cycles of imaging, as well as several steps designed to ensure a uniform calibration and to remove as many artefacts as possible.

In both cycles, MOST fan beam responses are converted to an image using the back projection algorithm (Perley 1979, Crawford 1984). The algorithm correctly forms the image in the selected co-ordinate system, applying appropriate corrections for precession and small geodetic misalignments in the baseline of the MOST. The images are formed initially in equatorial coordinates and the NCP projection (see Greisen 1983) to facilitate deconvolution. As a result of the extensive (u, v) coverage of a MOST observation, the synthesised point spread function is compact and relatively simple. Its first sidelobe has an amplitude of -8% , while the distant sidelobes all have amplitudes $< 1\%$.

The images are CLEANed using an image-plane algorithm similar to that described by Hogbom (1974). A source fitting algorithm (Crawford 1989) is then applied to provide a list of all of the compact sources. The list is sorted and amalgamated for the entire survey, and then used for (1) the modelling and removal of grating responses, (2) the iterative refinement of calibration parameters as described above, and (3) the production of a source catalogue to be presented in Paper II (in preparation).

The second and final synthesis of individual fields includes adjustment of the calibration factors, amelioration of grating rings (as an extension of the CLEAN process), the excision by Fourier filtering of any low-level solar interference, and the adaptive deconvolution of an image provided there is a strong, compact source ($S_{843} \geq 200$ mJy) near the centre of the field (Cram & Ye 1995). Typically, the calibration corrections at this final stage may change flux densities by $\sim 2\%$ and positions by $< 1''$.

The last step in forming survey images is to combine individual fields into a $3^\circ \times 3^\circ$ mosaic in Galactic co-ordinates. Each $3^\circ \times 3^\circ$ mosaic contains at least 16 component images. Before combination, every image is inspected visually, and areas containing evident artefacts are flagged for possible exclusion. After all component images have been flagged,

the mosaic is assembled. Sometimes, a flagged artefact will appear at the same position in all of the existing observations. The flagging process will then create a gap and the images are re-examined to select the least affected for inclusion.

3.3. Image Quality & Residual Artefacts

The images themselves (Figure 4) suggest that the steps summarised above have been very successful in providing high quality data in those parts of the Galactic plane devoid of bright, extended sources. In regions with bright, complex, spatially extended emission the images have a lower dynamic range. They are still of considerable value by virtue of their good sensitivity to low surface brightness and their relatively high angular resolution.

The residual artefacts in MOST images originate in several ways, and in general they can be readily distinguished from the sky emission by virtue of their position and structure. There are three *major* artefacts to consider, arising from (a) propagation effects, (b) grating responses, and (c) missing short spacings. The region of the sky near $l = 284.0^\circ$ [Figure 4(i)] illustrates one of the most difficult areas to image, and all three types of residual artefacts can be discerned. In addition, the projection of images to form the mosaic in (l, b) coordinates distorts the original synthesised beam shape, and the published images therefore have a position-dependent beam. We now consider each of these artefacts in turn.

3.3.1. Propagation effects

Propagation effects arise through time-dependent refractive gradients in the ionosphere and troposphere. These phenomena lead to bright and dark patterns which radiate from high brightness sources. The patterns are the direct consequence of the time-dependent distortion of the wavefront on its passage through the atmosphere, which this leads to small ($\sim 1 - 2''$ amplitude), time-dependent (~ 10 min time scales) apparent displacements in the positions of sources. Adaptive deconvolution (Cram & Ye 1995) has partially removed the effect but has been unable to improve the dynamic range beyond a ratio of 250 : 1.

3.3.2. Grating responses

The grating responses of the fan beams of the MOST are manifest in images as elliptical rings or arcs around bright sources, with minor and major radii $1.15^\circ n$ and $1.15^\circ n \operatorname{cosec} |\delta|$, respectively. Here, n is the order of the response. Most of the residual artefacts

correspond to $n = +1$, although for sources stronger than about 2.5 Jy a second and even a third ellipse may be detected. As explained by Amy & Large (1989), the amplitude of the grating response of the fan beams changes with the meridian distance of the field, and hence the amplitude of the synthesised ring varies across the field of view. In particular, the response is very weak near the field centre (i.e., from sources lying 1.15° from a field centre). Considerable efforts (involving real-time signal processing) were expended to reduce these responses as MGPS1 progressed. While these were successful, the cost is a residual response which is complex and therefore difficult to remove fully. The problem is exacerbated when the grating responses are produced by sources that are strong and complex.

3.3.3. Missing short spacings

The MOST does not measure the auto-correlation of its elements, nor does it measure correlations on baselines shorter than the inter-arm gap of 42.9λ . Hence, structures with angular sizes larger than $\sim 20' - 30'$ are not detected and in unCLEANed images all sources are surrounded by a ‘bowl’ of apparently negative flux density. The CLEAN algorithm can go some way to interpolating the unmeasured short spacings and thus to restoring the negative bowl (e.g. Schwarz 1984). However, small residual uncertainties in our knowledge of the actual MOST beam preclude the complete removal of this artefact in the presence of bright, extended sources that contain more than ≈ 100 Jy of flux density. An artefact related to the negative bowl arises when images containing such sources overlap at the mosaic. In this case, differences in the telescope beam and the depth of CLEANing in the two images may lead to systematic offsets between the local image base levels, manifest as a small, sharp step in the mosaiced image.

3.3.4. Position dependent synthesised beam

When the individual images comprising the survey were restored following the CLEAN process, the restoring beam was independent of position in the NCP projection. However, different images comprising a given mosaic have been restored with different beams, since the beam dimensions are set by the declination of the field centre (i.e., the phase centre). Consequently, the beam shape at any point in a MGPS1 mosaic is a linear combination of the set of beams for all the images contributing at that point (Sault, Killeen & Brouw 1996). This beam shape has been further distorted by the process of regridding to (l, b) coordinates. As a result, it is entirely inappropriate for users of the survey to attempt to deconvolve sources in the mosaics. Source fitting, especially of compact sources, should be

done on the original component images.

4. Results and prospects

The working product of the survey is a set of 37 mosaics, each covering an area of $3^\circ \times 3^\circ$ in Galactic co-ordinates. Each mosaic is composed of at least 16 calibrated individual fields, with simple averaging in overlapped regions. In this paper the images are further amalgamated into $9^\circ \times 3^\circ$ mosaics, shown in Figures 4(a) – 4(m), as greyscales within the range (white) -30 to (black) $+40$ mJy beam $^{-1}$. The peak amplitude of the stronger sources seen in the survey is often above 1 Jy, and they are thus burnt out in the images. However, the selected grayscale range exemplifies the capacity of the MOST to reveal faint, large-scale structure.

The mosaics show a panorama of the Galactic Plane characterised by a host of unresolved and small-diameter sources, together with a highly non-uniform population of extended and complex sources. Most of the small-diameter objects are background galaxies and their distribution appears to be uniform (Whiteoak 1992). There are also many extended objects which exhibit the typical morphology of radio galaxies (e.g., double-lobe, head-tail and wide-angle tail sources) distributed without any obvious clustering throughout the survey region, and probably all of these will also be background sources. Multi-wavelength studies of these extragalactic sources will help improve understanding of the sky in the Zone of Avoidance.

By contrast, there is a marked tendency for the host of large Galactic sources seen in the images to be apparently clustered into complexes. The most prominent of these complexes tend to occur at the longitudes associated with tangent directions to Galactic spiral arms (Mills 1959; Green 1974) and may well represent superpositions of several sources along the line of sight. The effect is especially obvious along the tangent direction at longitudes 312° [Figure 4(f)] and 332° [Figure 4(d)]. However, there are other complexes lying in directions not known to be associated with tangent point directions. Some of these have morphologies suggestive of large scale physical association within the complex. For example, there are large plumes and groupings which strongly suggest interactions at longitudes 317° [Figure 4(e)] and 327° [Figure 4(d)]. The images show many filaments extending over several degrees. It is not known whether these structures have a separate physical identity or are perturbations in the emission from larger, more homogeneous phases of the interstellar medium (ISM).

Multi-wavelength comparisons can be made between MGPS1 and the IRAS 60 μ m

survey. Thermal sources dominate the IRAS images and the ratio of the flux densities at 60 μ m and 843 MHz proves to be a powerful discriminant between thermal and non-thermal processes (Whiteoak & Green 1996; Taylor et al. 1996). Further insights will be gained when these data are related to the wide-field H α imaging surveys currently in progress at the Siding Spring Observatory (Buxton, Bessel & Watson 1998; Parker & Phillips 1998). Detailed correlations can also be explored with the overlapping portion of the 1.4 GHz NRAO-VLA Sky Survey (Condon et al. 1998), and with the 5 GHz Parkes-MIT-NRAO survey (Griffith & Wright 1993).

The MGPS1 can potentially reveal *variable* radio sources, from inspection of the regions of overlap between the 70' images. Any such variability will be detected in the process of developing a source catalogue, which is currently in preparation. Furthermore, a larger second epoch survey, MGPS2, is currently in progress to explore variability on longer time scales and to extend the surveyed region to higher galactic latitudes (Large et al. 1994; Green 1997, 1998). It is hoped the MGPS1 will form the basis for many individual source investigations as well as studies of large-scale structures in the ISM, including identification of relic SNRs and wind-blown bubbles of ionised gas. To assist in this work, $3 \times 3^\circ$ versions of the images displayed in this paper (together with subimages of selected objects, such as the supernova remnants described by Whiteoak & Green 1996) are available in FITS format from the website <http://www.astrop.physics.usyd.edu.au/MGPS>. The original images, necessary for quantitative source fitting, may also be downloaded from this site.

The Molonglo Observatory Site Manager, D. Campbell-Wilson, and the technical staff, J. Webb, M. White and B. Smithers have made a considerable contribution to the success of this project and we warmly acknowledge their dedication and skill. B. Piestrzynski analysed and organised the data archive and managed the data processing with outstanding care and commitment. Software used in the data reduction has been developed with assistance from several astronomers, including J. Reynolds, S. Amy, A. Gray and V. McIntyre, and we gratefully acknowledge their contribution. The MOST is operated with the support of the Australian Research Council and the Science Foundation for Physics within the University of Sydney.

REFERENCES

Amy, S. & Large, M. I. 1989, *Publ. Astr. Soc. Australia*, 8, 308

Bock, C.-J., Turtle, A. J. & Green, A. J. 1998, *AJ*, (in press)

Buxton, M., Bessell, M. & Watson, B. 1998, *Publ. Astr. Soc. Australia*, 15, 24

Campbell-Wilson, D. & Hunstead, R. W. 1994, *Publ. Astr. Soc. Australia*, 11, 33

Condon, J. J., Cotton, W. D., Greisen, E. W., Yin, Q. F., Perley, R. A., Taylor, G. B. & Broderick, J. J. 1998, *AJ*, 115, 1693

Cram, L. E. & Ye, T. 1995, *Australian J. Phys.*, 48, 113

Crawford, D. F. 1984, in *Indirect Imaging*, ed Roberts, J. A., (Cambridge: Cambridge Uni. Press), 373

Crawford, D. F. 1989, *Publ. Astr. Soc. Australia*, 8, 86

Duncan, A. R., Stewart, R. T., Haynes, R. F. & Jones, K. L. 1995, *MNRAS*, 277, 36

Goss, W. M. & Shaver, P. A. 1970, *Australian J. Phys. Astrop. Suppl.*, 14, 1

Gray, A. D. 1994a, *MNRAS*, 270, 822

Gray, A. D. 1994b, *MNRAS*, 270, 835

Gray, A. D. 1994c, *MNRAS*, 270, 847

Gray, A. D. 1994d, *MNRAS*, 270, 861

Green, A. J. 1974, *A&AS*, 18, 267

Green, A. J. 1997, *Publ. Astr. Soc. Australia*, 14, 73

Green, A. J. 1998, *PASP Conf. Series* (in press)

Greisen, E. W. 1983, AIPS Memo No 27, (Charlottesville, National Radio Astronomy Observatory)

Griffith, M. R. & Wright, A. E. 1993, *AJ*, 105, 1666

Haynes, R. F., Caswell, J. L. & Simons, L. W. J. 1978, *Australian J. Phys. Astrop. Suppl.*, 48, 1

Hunstead, R. W. 1991, *Australian J. Phys.*, 44, 743

Hogbom, J. A. 1974, *A&AS*, 15, 417

Large, M. I., Campbell-Wilson, D., Cram, L. E., Davison, R. G. & Robertson, J. G. 1994, *Publ. Astr. Soc. Australia*, 11, 44

Mills, B. Y. 1959, in *The Paris Sympopsium on Radio Astronomy*, ed Bracewell, R. N., (Stanford: Stanford Uni. Press), 431

Mills, B. Y. 1981, *Publ. Astr. Soc. Australia*, 4, 156

Parker, Q. A. & Phillipps 1998, *Publ. Astr. Soc. Australia*, 15, 28

Perley, R. A. 1979, *AJ*, 84, 1443

Robertson, J. G. 1991, *Australian J. Phys.*, 44, 729

Sault, R. J., Staveley-Smith, L. & Brouw, W. N. 1996, *A&A*, 120, 375

Schwarz, 1984, in *Indirect Imaging*, ed. J. A. Roberts, p255

Shaver, P. A. & Goss, W. M. 1970, *Australian J. Phys. Astrop. Suppl.*, 14, 77

Staveley-Smith, L., Juraszek, S., Koribalski, B., et al., 1998, *AJ*, in press, Dec 1998

Taylor, A. R., Goss, W. M., Coleman, P. H., van Leeuwen, J. & Wallace, B. J. 1996, *ApJS*, 107, 239

Whiteoak, J. B. Z. 1992, *A&A*, 262, 251

Whiteoak, J. B. Z. & Green, A. J. 1996, *A&AS*, 118, 329

Whiteoak, J. B. Z., Large, M. I., Cram, L. E., Piestrzynski, B. 1989, *Publ. Astr. Soc. Australia*, 8, 176

Fig. 1.— Definition of the tilt and meridian distance (MD) co-ordinates of a point P . This is the natural system for the MOST. The directions N and W point to North and West, respectively, and Z is towards the Zenith.

Fig. 2.— Plot showing the location of all the component fields observed as part of MGPS1. Pointing centres associated with the Galactic Centre (Gray 1994a,b,c,d) and Vela (Bock et al. 1998) complementary surveys are also shown.

Fig. 3.— Flow chart showing the process used to produce the final product of the survey, namely $3^\circ \times 3^\circ$ mosaics in Galactic co-ordinates.

Fig. 4.— Large mosaics, $9^\circ \times 3^\circ (l \times b)$, of the Galactic plane covered by MGPS1. The greyscale has been compressed to the range -30 to $+40$ mJy beam $^{-1}$ to show more clearly the faint, extended structure. The full dynamic range is available in the electronic version of the data.

Table 1: Technical specifications of the MOST

Centre frequency	843 MHz ($\lambda = 36$ cm)
Bandwidth	3 MHz
Polarization	RHC (IEEE)
Declination range	-90° to $\approx -30^\circ$
Synthesised beam	$43'' \times 43''$ cosec $ \delta $
Field size (MGPS1)	$70' \times 70'$ cosec $ \delta $
Noise after 12 h	1 - 2 mJy beam $^{-1}$ (1 σ)
Surface brightness sensitivity	≈ 1 K (1 σ)
Dynamic range (best)	250:1

500pt760pt

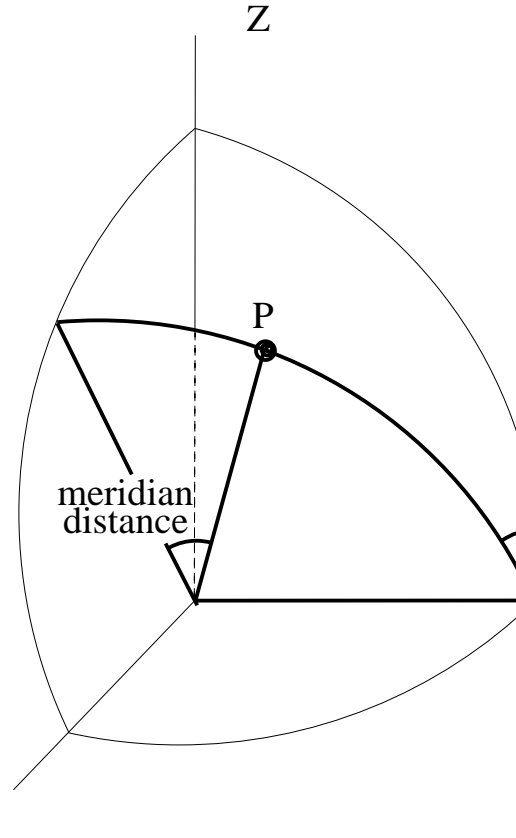


Figure 1. Definition of the tilt and meridian distance co-ordinates of a point P . This is the natural system for the MOST. N and W point to North and West, respectively, and Z is the Zenith.

760pt

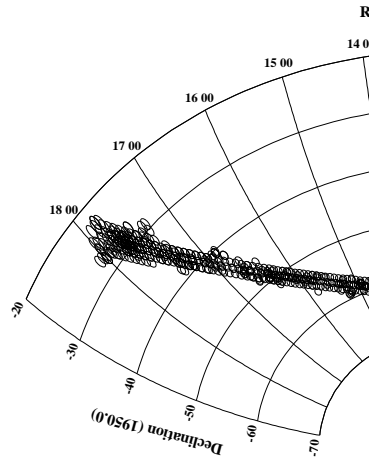


Figure 2. Plot showing the location of all the component fields observed as part of MGPS1. Pointing centres associated with the Galactic Centre (Gray 1994a,b,c,d) and Vela (Bock et al. 1998) complementary surveys are also shown.

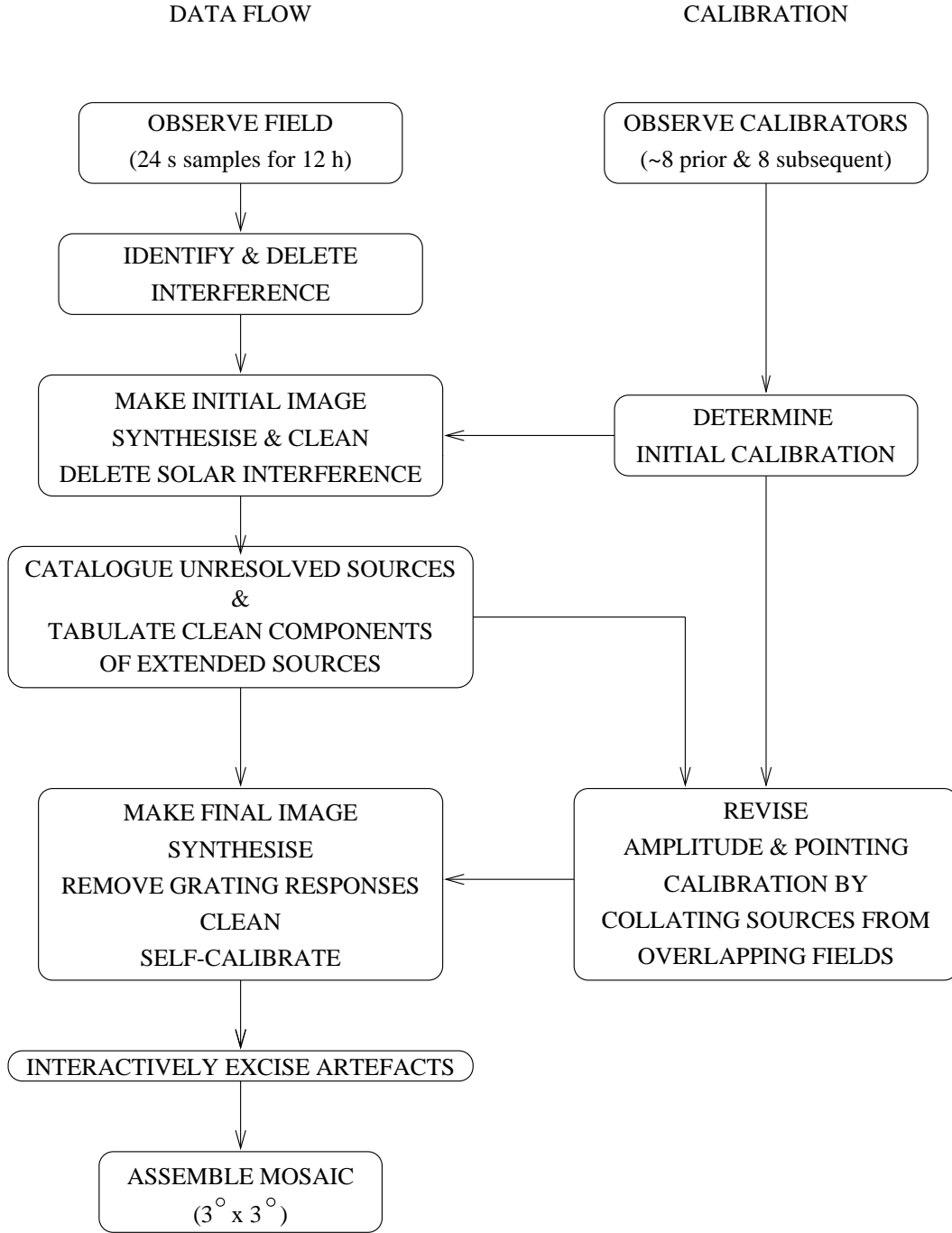


Figure 3. Plot showing the location of all the component fields observed as part of MGPS1. Pointing centres associated with the Galactic Centre (Gray 1994a,b,c,d) and Vela (Bock et al. 1998) complementary surveys are also shown.

TABLE 1
LOG OF OBSERVATIONS OF MGPS-1

Field Centre	α (J2000)	δ (J2000)	Date	Field Centre	α (J2000)	δ (J2000)	Date	
G245.25-0.9	07 52 17.2	-28 52 32	1990 Jan 30	G303.75+0.0	12 58 36.7	-62 51 37	1989 Apr 14	
G245.25+0.9	07 59 17.2	-27 56 33	1990 Jan 14	G303.8-0.7	12 59 07.0	-63 36 11	1991 Apr 19	
			1991 Sep 28	G304.12-0.8	13 02 08.9	-63 41 08	1990 Mar 14	
G245.75+0.0	07 56 59.1	-28 50 20	1987 Feb 02	G304.125-0.9	13 02 13.7	-63 44 48	1989 Apr 16	
G246.25-0.9	07 54 38.6	-29 43 59	1990 Jan 15	G304.125+0.9	13 01 35.2	-61 56 54	1989 Apr 30	
G246.25+0.9	08 01 40.8	-28 47 32	1990 Jan 16	G304.5+0.0	13 05 10.8	-62 49 48	1991 Apr 14	
			1992 Jan 31	G304.875-0.9	13 08 59.7	-63 42 20	1989 Apr 19	
G246.75+0.0	07 59 22.9	-29 41 29	1989 Jan 17	G304.875+0.9	13 07 57.2	-61 54 34	1992 May 01	
G247.25-0.9	07 57 02.5	-30 35 17	1991 Sep 29	G305.25+0.0	13 11 43.8	-62 46 49	1983 Apr 18	
G247.25+0.9	08 04 06.9	-29 38 22	1991 Sep 08	G305.625-0.9	13 15 44.2	-63 38 41	1986 Apr 09	
G247.75+0.0	08 01 49.2	-30 32 29	1987 Feb 04	G305.625+0.9	13 14 18.0	-61 51 08	1993 Mar 22	
G248.25-0.9	07 59 28.9	-31 26 26	1991 Sep 22	G305.9+1.0	13 16 58.7	-61 45 49	1991 Apr 03	
G248.25+0.9	08 06 35.5	-30 29 01	1991 Oct 04	G306.0+0.0	13 18 15.3	-62 42 43	1993 Apr 03	
G248.75+0.0	08 04 18.0	-31 23 17	1991 Nov 01	G306.375-0.9	13 22 26.7	-63 33 51	1989 Apr 23	
G249.25-0.9	08 01 57.8	-32 17 25	1991 Sep 21	G306.375+0.9	13 20 37.1	-61 46 35	1989 May 07	
G249.25+0.9	08 09 06.8	-31 19 28	1991 Oct 12	G306.4+0.1	13 21 17.4	-62 35 43	1992 Jun 26	
G249.75+0.0	08 06 49.6	-32 13 55	1991 Nov 02	G306.75+0.0	13 24 44.7	-62 37 29	1989 May 03	
G250.25-0.9	08 04 29.5	-33 08 13	1991 Sep 27	G307.125-0.9	13 29 06.7	-63 27 53	1990 Mar 18	
G250.25+0.9	08 11 40.9	-32 09 44	1991 Oct 13	G307.125+0.9	13 26 54.1	-61 40 58	1984 Apr 02	
G250.75+0.0	08 09 23.8	-33 04 22	1991 Nov 23	G307.5+0.0	13 31 11.5	-62 31 07	1983 Apr 20	
G251.25-0.9	08 07 04.1	-33 58 50	1991 Oct 06	G307.875-0.9	13 35 43.7	-63 20 45	1990 Mar 20	
G251.25+0.9	08 14 17.9	-32 59 47	1991 Oct 18	G307.875+0.9	13 33 08.6	-61 34 15	1990 Mar 19	
			1991 Nov 15	G308.25+0.0	13 37 35.4	-62 23 39	1986 Apr 07	
G251.75+0.0	08 12 01.3	-33 54 36	1991 Nov 24	G308.625-0.9	13 42 17.2	-63 12 30	1988 Apr 14	
G252.25-0.9	08 09 41.8	-34 49 15	1991 Jan 07	G308.625+0.9	13 39 20.2	-61 26 28	1983 Apr 21	
G252.25+0.9	08 16 57.9	-33 49 37	1991 Jan 09	G309.0+0.0	13 43 55.9	-62 15 06	1983 Apr 26	
G252.75+0.0	08 14 41.8	-34 44 37	1991 Nov 16	G309.2-0.4	13 46 30.3	-62 35 00	1991 Apr 11	
G253.25-0.9	08 12 22.6	-35 39 27	1990 Jan 17	G309.375-0.9	13 48 46.7	-63 03 08	1985 Apr 11	
G253.25+0.9	08 19 41.2	-34 39 14	1991 Jan 15	G309.375+0.9	13 45 28.5	-61 17 38	1986 May 01	
G253.75+0.0	08 17 25.5	-35 34 25	1992 Mar 29	G309.7+1.7	13 46 45.5	-60 24 59	1994 Mar 28	
G254.25-0.9	08 15 06.7	-36 29 27	1990 Jan 18	G309.75+0.0	13 50 12.5	-62 05 29	1985 Feb 02	
G254.25+0.9	08 22 27.8	-35 28 36	1991 Jan 19	G310.0+0.5	13 51 30.4	-61 34 50	1991 Apr 15	
G254.75+0.0	08 20 12.7	-36 23 59	1984 Feb 02	G310.125-0.9	13 55 11.8	-62 52 40	1988 Apr 24	
G255.25-0.9	08 17 54.3	-37 19 13	1991 Oct 20	G310.125+0.9	13 51 33.1	-61 07 46	1988 Apr 25	
G255.25+0.9	08 25 17.9	-36 17 42	1991 Aug 11	G310.5+0.0	13 56 25.0	-61 54 48	1985 Apr 15	
G255.75+0.0	08 23 03.4	-37 13 18	1986 Feb 10	G310.8+0.0	13 59 05.5	-62 10 34	1991 Apr 16	
G256.25-0.9	08 20 45.6	-38 08 44	1991 Jan 17	G310.875-0.9	14 01 32.2	-62 41 09	1992 Jun 12	
G256.25+0.9	08 28 11.6	-37 06 33	1991 Aug 25	G310.875+0.9	13 57 33.7	-60 56 52	1986 May 07	
G256.75+0.0	08 25 57.9	-38 02 21	1986 Feb 11	G311.1+0.2	14 00 31.6	-61 34 41	1990 Apr 05	
G257.25-0.9	08 23 40.7	-38 58 00	1991 Aug 10	G311.25+0.0	14 02 33.0	-61 43 05	1993 Apr 09	
G257.25+0.9	08 31 09.2	-37 55 07	1991 Aug 24	G311.625-0.9	14 07 47.4	-62 28 34	1985 Apr 17	
G257.75+0.0	08 28 56.3	-38 51 08	1986 Feb 12	G311.625+0.9	14 03 30.1	-60 44 59	1985 Apr 18	
G258.25-0.9	08 26 39.9	-39 47 00	1990 Jan 19	G312.0-3.0	14 20 52.1	-64 13 44	1995 Sep 02	
G258.25+0.9	08 34 10.8	-38 43 24	1992 Feb 03	G312.0+0.0	14 08 36.1	-61 30 21	1984 Apr 03	
G258.75+0.0	08 31 58.8	-39 39 38	1986 Feb 13				1990 Apr 15	
G259.25-0.9	08 29 43.2	-40 35 42	1989 Jan 19	G312.375-0.9	14 13 57.3	-62 14 57	1988 Apr 26	
G259.25+0.9	08 37 16.6	-39 31 22	1989 Jan 18	G312.375+0.9	14 09 21.9	-60 32 06	1991 Apr 05	
G259.75+0.0	08 35 05.7	-40 27 49	1986 Feb 18	G312.5-0.2	14 13 04.3	-61 34 13	1990 Apr 09	
G260.25-0.9	08 32 51.0	-41 24 07	1992 Mar 01	G312.75+0.0	14 14 34.1	-61 16 37	1986 Apr 30	
G260.25+0.9	08 40 26.8	-40 19 00	1994 Jan 26	G313.125-0.9	14 20 01.4	-62 00 21	1990 Apr 11	
G260.75+0.0	08 38 17.0	-41 15 41	1986 Feb 20	G313.125+0.9	14 15 08.8	-60 18 16	1990 Apr 10	
G261.25-0.9	08 36 03.5	-42 12 13	1988 Feb 19				1992 Mar 25	
G261.25+0.9	08 43 41.5	-41 06 18	1984 Feb 03	G313.5+0.0	14 20 26.8	-61 01 56	1990 Apr 29	
G261.75+0.0	08 41 33.1	-42 03 13	1989 Jan 20	G313.875-0.9	14 25 59.6	-61 44 46	1990 Apr 14	
G262.25-0.9	08 39 20.8	-42 59 58	1988 Feb 21	G313.875+0.9	14 20 50.7	-60 03 30	1990 Apr 28	
G262.25+0.9	08 47 01.1	-41 53 14	1988 Feb 20	G314.25+0.0	14 26 13.9	-60 46 18	1993 Apr 18	
G262.75-1.8	08 37 03.8	-43 56 34	1992 Jan 29	N	G314.625-0.9	14 31 51.6	-61 28 15	1990 Apr 30
G262.75+0.0	08 44 54.1	-42 50 23	1992 Feb 12	G314.625+0.9	14 26 27.4	-59 47 49	1991 Apr 17	
G263.0-0.2	08 44 53.5	-43 10 58	1990 Feb 09	N	G315.0+0.0	14 31 55.2	-60 29 45	1993 Apr 13
G263.25-0.9	08 42 43.1	-43 47 23	1992 Feb 07	G315.375-0.9	14 37 37.4	-61 10 48	1990 Apr 19	
G263.25+0.9	08 50 25.6	-42 39 48	1988 Feb 22	G315.375+0.9	14 31 58.6	-59 31 15	1990 May 01	
G263.75+0.0	08 48 20.2	-43 37 11	1992 Feb 15	G315.4-2.4	14 42 56.2	-62 29 45	1994 Apr 29	
G264.25-0.9	08 46 10.8	-44 34 25	1992 Feb 14	G315.5-0.1	14 35 46.5	-60 23 05	1992 Dec 06	
G264.25+0.9	08 53 55.4	-43 25 58	1989 Jan 27	G315.75+0.0	14 37 30.7	-60 12 18	1985 Feb 01	
G264.75+0.0	08 51 51.8	-44 23 35	1992 Feb 16	G316.125-0.9	14 43 16.7	-60 52 27	1990 May 04	
G265.25-0.9	08 49 44.1	-45 21 04	1989 Jan 29	G316.125+0.9	14 37 24.3	-59 13 48	1990 May 02	
G265.25+0.9	08 57 30.6	-44 11 42	1984 Feb 07	G316.5+0.0	14 43 00.0	-59 53 59	1993 Apr 15	
G265.75+0.0	08 55 29.0	-45 09 34	1989 Jan 29	G316.875-0.9	14 48 49.4	-60 33 15	1990 May 06	
G266.25-0.9	08 53 23.2	-46 07 18	1989 Jan 31				1993 Apr 14	
G266.25+0.9	09 01 11.5	-44 57 00	1989 Jan 30	G316.875+0.9	14 42 44.3	-58 55 32	1990 May 03	
G266.75+0.0	08 59 12.1	-45 55 07	1993 Mar 14	G316.9-0.1	14 45 18.5	-59 49 38	1994 Apr 18	
G267.25-0.9	08 57 08.5	-46 53 05	1990 Jan 21	N	G317.0+0.1	14 46 18.2	-59 32 36	1990 Apr 20
G267.25+0.9	09 04 58.3	-45 41 49	1990 Jan 22	G317.2+1.2	14 43 44.4	-58 32 43	1991 Apr 08	
G267.75+0.0	09 03 01.3	-46 40 11	1990 Jan 23	G317.25+0.0	14 48 23.3	-59 34 50	1984 Apr 04	
G268.25-0.9	09 01 00.1	-47 38 25	1992 Mar 02				1993 Apr 16	
G268.25+0.9	09 08 51.3	-46 26 10	1990 Jan 24	G317.625-0.9	14 54 15.5	-60 13 13	1990 May 11	
G268.75+0.0	09 06 57.0	-47 24 47	1990 Jan 25	G317.625+0.9	14 47 58.6	-58 36 26	1990 May 05	
G269.25-0.9	09 04 58.4	-48 23 16	1985 Jan 31	G318.0+0.0	14 53 40.3	-59 14 53	1990 May 10	
G269.25+0.9	09 12 50.7	-47 09 59	1990 Jan 27				1993 Apr 30	
G269.75+0.0	09 10 59.4	-48 08 51	1990 Feb 28	G318.3-0.1	14 55 20.5	-59 14 09	1992 Mar 30	
G270.25-0.9	09 09 03.7	-49 07 35	1990 Feb 01	G318.3+0.1	14 55 19.9	-59 02 09	1990 Apr 21	
G270.25+0.9	09 16 56.8	-47 53 16	1991 Feb 28	G318.375-0.9	14 59 35.0	-59 52 22	1990 May 13	
G270.75+0.0	09 15 08.7	-48 52 22	1991 Feb 05	G318.375+0.9	14 53 07.1	-58 16 32	1990 May 07	
G271.125-0.9	09 12 44.3	-49 45 56	1991 Feb 27	G318.75+0.0	14 58 51.1	-58 54 08	1986 May 11	
G271.125+0.9	09 20 37.9	-48 30 39	1991 Feb 12	G319.0+0.5	14 59 34.1	-58 17 56	1993 May 21	
G271.5+0.0	09 18 20.5	-49 24 38	1991 Jul 28	G319.1-0.1	15 01 51.4	-58 46 49	1991 May 10	

TABLE 1—Continued

Field Centre	α (J2000)	δ (J2000)	Date	Field Centre	α (J2000)	δ (J2000)	Date
G271.875-0.9	09 15 58.0	-50 18 26	1991 Feb 07	G319.125-0.9	15 04 47.7	-59 30 44	1990 May 14
G271.875+0.9	09 23 51.8	-49 02 21	1991 Jun 22	G319.125+0.9	14 58 09.7	-57 55 53	1990 May 12
G272.25+0.0	09 21 36.6	-49 56 34	1991 Feb 15	G319.5+0.0	15 03 55.7	-58 32 37	1993 May 01
G272.625-0.9	09 19 16.2	-50 50 37	1991 Feb 11	G319.875-0.9	15 09 53.8	-59 08 21	1988 May 13
G272.625+0.9	09 27 09.9	-49 33 41	1991 Feb 20	G319.875+0.9	16 21 03.9	-49 57 14	1984 Apr 05
G273.0+0.0	09 24 56.9	-50 28 08	1991 Feb 19	G320.25+0.0	15 08 53.9	-58 10 22	1992 Mar 28
G273.375-0.9	09 22 38.8	-51 22 26	1991 Feb 17	G320.4-1.2	15 14 36.6	-59 05 09	1990 Jun 02
G273.375+0.9	09 30 32.2	-50 04 39	1991 Feb 23	G320.5-1.5	15 16 28.1	-59 21 03	1992 Sep 26
G273.75+0.0	09 28 21.8	-50 59 21	1991 Feb 21	G320.625-0.9	15 14 53.1	-58 45 14	1985 May 08
G274.125-0.9	09 26 06.1	-51 53 54	1984 Feb 15	G320.625+0.9	15 07 57.2	-57 12 22	1987 May 01
G274.125+0.9	09 33 59.0	-50 35 14	1990 Feb 07	G320.7-1.8	15 18 59.2	-59 26 54	1993 Mar 29
G274.5+0.0	09 31 51.3	-51 30 11	1990 Feb 05	G320.7+1.1	15 07 48.2	-57 01 30	1992 Mar 27
G274.875-0.9	09 29 38.3	-52 24 59	1986 Mar 03	G320.8-1.6	15 19 18.7	-59 14 53	1992 Apr 06
G274.875+0.9	09 37 30.4	-51 05 26	1990 Feb 08	G321.0+0.0	15 13 45.9	-57 47 25	1992 Apr 17
G275.25+0.0	09 35 25.5	-52 00 37	1990 Feb 12	G321.375-0.9	15 19 45.9	-58 21 26	1986 May 19
G275.625-0.9	09 33 15.4	-52 55 39	1990 Feb 13	G321.375+0.9	15 12 42.2	-56 49 33	1984 Apr 09
G275.625+0.9	09 41 06.3	-51 35 12	1986 Mar 04	G321.4-0.5	15 18 24.4	-58 00 56	1991 May 01
G276.0+0.0	09 39 04.6	-52 30 38	1990 Feb 14	G321.75+0.0	15 18 31.7	-57 23 46	1992 Apr 03
G276.375-0.9	09 36 57.6	-53 25 55	1990 Feb 16	G322.125-0.9	15 24 32.1	-57 56 57	1987 May 07
G276.375+0.9	09 44 47.1	-52 04 33	1990 Feb 17	G322.125+0.9	15 17 21.3	-56 26 04	1984 Apr 11
G276.75+0.0	09 42 48.7	-53 00 13	1990 Feb 15	G322.2+0.6	15 18 40.4	-56 38 55	1994 Apr 19
G277.125-0.9	09 40 45.1	-53 55 45	1990 Feb 18	G322.5+0.0	15 23 11.3	-56 59 28	1992 Apr 07
G277.125+0.9	09 48 32.7	-52 33 27	1990 Feb 19	G322.7-0.2	15 25 23.4	-57 00 33	1991 Apr 18
G277.5+0.0	09 46 38.0	-53 29 21	1990 Feb 20	G322.875-0.9	15 29 11.8	-57 31 49	1987 May 08
G277.875-0.9	09 44 38.0	-54 25 08	1986 Mar 05	G322.875+0.9	15 21 54.6	-56 01 56	1984 Apr 10
G277.875+0.9	09 52 23.4	-53 01 54	1986 Mar 10	G323.25+0.0	15 27 44.9	-56 34 32	1986 May 22
G278.25+0.0	09 50 32.5	-53 58 01	1990 Feb 22	G323.625-0.9	15 33 45.1	-57 06 04	1987 May 14
G278.625-0.9	09 48 36.5	-54 54 02	1990 Feb 23	G323.625+0.9	15 26 22.2	-55 37 11	1987 May 25
G278.625+0.9	09 56 19.2	-53 29 51	1990 Feb 26	G324.0+0.0	15 33 12.4	-56 08 59	1992 Apr 08
G279.0+0.0	09 54 32.4	-54 26 12	1990 Feb 27	G324.375-0.9	15 38 12.2	-56 39 44	1987 May 18
			1991 Mar 04	G324.375+0.9	15 30 44.1	-55 11 49	1987 May 26
G279.375-0.9	09 52 40.6	-55 22 27	1991 Mar 28	G324.75+0.0	15 36 34.0	-55 42 51	1987 May 28
G279.375+0.9	10 00 20.2	-53 57 19	1991 Mar 08	G325.125-0.9	15 42 33.0	-56 12 48	1987 May 27
G279.75+0.0	09 58 37.8	-54 53 53	1991 Mar 07	G325.125+0.9	15 35 00.4	-54 45 53	1988 May 07
G280.125-0.9	09 56 50.5	-55 50 22	1991 Mar 05	G325.4+0.9	15 36 49.5	-54 39 53	1991 May 02
G280.125+0.9	10 04 26.5	-54 24 15	1992 Feb 17	G325.5+0.0	15 40 49.7	-55 16 09	1987 May 29
G280.5+0.0	10 02 48.9	-55 21 02	1989 Feb 04	G325.875-0.9	15 46 47.8	-55 45 20	1990 May 19
G280.875-0.9	10 01 06.4	-56 17 44	1993 Mar 28	G325.875+0.9	15 39 11.2	-54 19 24	1990 May 16
G280.875+0.9	10 08 38.3	-54 50 38	1988 Mar 30	G326.25+0.0	15 44 59.7	-54 48 54	1990 May 18
			1989 Feb 06	G326.3-1.6	15 52 54.8	-56 13 25	1992 Apr 09
G281.25+0.0	10 07 05.7	-55 47 38	1986 Mar 11	G326.625-0.9	15 50 56.7	-55 17 20	1991 Apr 23
G281.625-0.9	10 05 28.4	-56 44 33	1985 Feb 04	G326.625+0.9	15 43 16.5	-53 52 22	1990 May 17
G281.625+0.9	10 12 55.6	-55 16 28	1988 Mar 31				1992 Jul 08
G282.0-1.8	10 03 43.4	-57 39 26	1991 Mar 11	N	G327.0+0.0	15 49 04.1	-54 21 08
G282.0-1.2	10 06 44.3	-57 12 41	1994 Mar 01	N	G327.375-0.9	15 54 59.8	-54 48 50
G282.0+0.0	10 11 28.3	-56 13 40	1986 Mar 12	G327.375+0.9	15 47 16.6	-53 24 49	1990 May 20
G282.375-0.9	10 09 56.6	-57 10 48	1985 Feb 14	G327.75+0.0	15 53 03.1	-53 52 51	1993 Apr 20
G282.375+0.9	10 17 18.5	-55 41 43	1989 Feb 08	G328.125-0.9	15 58 57.2	-54 19 50	1991 Apr 27
G282.75+0.0	10 15 56.9	-56 39 06	1988 Mar 14	G328.125+0.9	15 51 11.4	-52 56 46	1991 Apr 25
G283.125-0.9	10 14 31.0	-57 36 26	1985 Feb 19	G328.5+0.0	15 56 56.6	-53 24 06	1993 Apr 21
G283.125+0.9	10 21 47.1	-56 06 22	1987 Mar 10	G328.6-0.4	15 58 51.6	-53 38 33	1991 Jun 01
G283.5+0.0	10 20 31.5	-57 03 56	1993 Mar 01	G328.875-0.9	16 02 49.1	-53 50 22	1989 May 04
G283.875-0.9	10 19 11.9	-58 01 27	1992 Mar 03	G328.875+0.9	15 55 01.2	-52 28 15	1991 Apr 26
G283.875+0.9	10 26 21.5	-56 30 22	1987 Mar 09	G329.25+0.0	16 00 44.9	-52 54 53	1992 May 04
G284.0+0.8	10 26 33.3	-56 40 19	1991 Mar 13	N	G329.625-0.9	16 06 35.6	-53 20 27
G284.25+0.0	10 25 12.3	-57 28 07	1983 Mar 10	N	G329.625+0.9	15 58 45.9	-51 59 15
G284.3-0.4	10 24 20.5	-57 49 15	1994 Mar 02	N	G329.9+0.5	16 01 48.0	-52 08 22
G284.4-0.5	10 24 35.6	-57 56 43	1987 Apr 06	N	G330.0+0.0	16 04 28.1	-52 25 13
			1987 Apr 14	N			1993 Apr 22
G284.625-0.9	10 23 59.3	-58 25 48	1985 Feb 25	N	G330.2-0.3	16 06 49.8	-52 28 03
G285.625+0.0	10 27 35.1	-57 40 00	1984 Mar 31	N	G330.375-0.9	16 10 16.9	-52 50 07
G284.625+0.9	10 31 01.7	-56 53 44	1993 Mar 03	N	G330.375+0.9	16 02 25.8	-51 29 50
G285.0+0.0	10 29 59.2	-57 51 38	1992 Mar 04	N	G330.75+0.0	16 08 06.3	-51 55 07
G285.37+0.1	10 32 53.9	-57 55 29	1992 Mar 05	N	G331.125-0.9	16 13 53.1	-52 19 22
G285.375-0.9	10 28 53.3	-58 49 29	1993 Mar 02	N	G331.125+0.9	16 06 00.9	-50 59 58
G285.375+0.9	10 35 47.7	-57 16 26	1993 Mar 05	N	G331.5+0.0	16 11 39.7	-51 24 37
G285.4+0.0	10 32 53.7	-58 05 29	1991 Mar 15	N			1993 Apr 25
			1991 Apr 02	N	G331.875-0.9	16 17 24.4	-51 48 13
G285.5-1.0	10 29 20.8	-58 55 24	1991 Mar 14	N	G331.875+0.9	16 09 31.4	-50 29 43
G285.75+0.0	10 34 52.3	-58 14 28	1993 Mar 04	N	G332.25+0.0	16 15 08.3	-50 53 43
G286.125-0.9	10 33 53.9	-59 12 28	1988 Mar 21	N	G332.625-0.9	16 20 50.9	-51 16 41
G286.125+0.9	10 40 39.6	-57 38 25	1989 Feb 11	N	G332.625+0.9	16 12 57.4	-49 59 03
G286.29-0.8	10 35 33.1	-50 10 34	1992 Feb 23	N	G333.0+0.0	16 18 32.3	-50 22 26
G286.5-2.4	10 30 38.4	-60 39 26	1990 Mar 01	N	G333.375-0.9	16 24 12.7	-50 44 48
G286.5+0.0	10 39 51.7	-58 36 34	1985 Feb 27	N	G333.375+0.9	16 16 18.9	-49 28 01
G286.6+0.0	10 40 32.3	-58 36 35	1990 Apr 07	N	G333.5+0.5	16 22 46.9	-50 22 00
G286.7-1.2	10 36 12.5	-59 45 35	1990 Mar 02	N	G333.75+0.0	16 21 51.9	-49 50 48
G286.875-0.9	10 39 01.1	-59 34 43	1985 Mar 01	N	G334.125-0.9	16 27 30.0	-50 12 34
G286.875+0.9	10 45 37.4	-57 59 41	1989 Feb 12	N	G334.125+0.9	16 19 36.2	-48 56 37
G287.17-1.6	10 38 22.5	-60 19 38	1992 Feb 24	N	G334.4+0.7	16 21 43.2	-48 57 04
G287.25+0.0	10 44 57.4	-58 57 57	1985 Mar 05	N	G334.5+0.0	16 25 07.1	-49 18 48
G287.5+0.6	10 48 29.9	-58 32 53	1990 Mar 07	N			1992 Jul 16
G287.6-2.1	10 39 11.9	-60 59 39	1990 Mar 03	N	G334.875-0.9	16 30 42.9	-49 39 59
G287.625-0.9	10 44 15.1	-59 56 12	1992 Feb 19	N	G334.875+0.9	16 22 49.4	-48 24 52
			1993 Mar 08	N	G335.25+0.0	16 28 18.2	-48 46 29
G287.625+0.9	10 50 41.0	-58 20 12	1989 Feb 13				1989 May 12

TABLE 1—Continued

Field Centre	α (J2000)	δ (J2000)	Date	Field Centre	α (J2000)	δ (J2000)	Date	
G288.0+0.0	10 50 09.3	-59 18 34	1993 Mar 09	G335.75-0.9	16 34 22.7	-49 01 35	1989 May 15	
G288.35-0.9	10 49 27.9	-60 15 54	1992 Feb 25	N	G335.75+0.9	16 26 29.6	-47 47 24	1989 May 11
G288.375-0.9	10 49 35.7	-60 16 54	1992 Feb 26		G336.0-0.8	16 34 44.5	-48 46 12	1991 Apr 30
G288.375+0.9	10 55 50.6	-58 39 57	1989 Feb 14		G336.25+0.0	16 32 26.6	-48 02 53	1993 May 11
G288.5-1.6	10 47 46.1	-60 59 52	1990 Mar 06	N	G336.5-1.3	16 39 14.3	-48 45 49	1992 May 06
G288.5-0.2	10 53 10.5	-59 45 59	1990 Mar 08	N	G336.75-0.9	16 38 27.0	-48 17 11	1993 Apr 28
G288.75+0.0	10 55 27.5	-59 38 23	1985 Mar 13		G336.75+0.9	16 30 34.8	-47 04 03	1993 May 27
G289.125-0.9	10 55 03.0	-60 36 48	1989 Feb 26		G337.25+0.0	16 36 28.0	-47 18 44	1990 Jun 08
G289.125+0.9	11 01 05.9	-58 58 54	1989 Feb 17		G337.5+1.6	16 30 07.5	-46 01 30	1992 May 05
G289.5+0.0	11 00 51.9	-59 57 23	1989 Feb 16		G337.75-0.9	16 42 24.4	-47 32 17	1993 Jun 01
G289.875-0.9	11 00 37.0	-60 55 51	1983 Mar 14		G337.75+0.9	16 34 33.4	-46 20 09	1989 May 18
			1989 Feb 18		G338.1+0.1	16 39 19.7	-46 32 53	1990 Jun 09
G289.875+0.9	11 06 27.0	-59 17 02	1989 Feb 19		G338.25+0.0	16 40 22.8	-46 34 05	1992 Apr 16
G289.9+0.0	11 03 35.0	-60 06 11	1991 Mar 22	N	G338.75-0.9	16 46 15.1	-46 46 53	1989 May 23
G290.0-1.1	11 00 37.3	-61 10 08	1991 Mar 19	N	G338.75+0.9	16 38 25.5	-45 35 45	1993 May 12
G290.25+0.0	11 06 22.4	-60 15 32	1989 Feb 20		G339.2-0.6	16 46 39.8	-46 15 23	1991 May 16
G290.5+0.1	11 08 27.3	-60 16 16	1991 Mar 25	N	G339.2+0.5	16 41 37.6	-45 30 44	1991 Jun 02
G290.625-0.9	11 06 17.5	-61 14 02	1992 Jun 13		G339.25+0.0	16 44 11.2	-45 48 56	1992 Apr 20
G290.625+0.9	11 11 53.7	-59 34 19	1984 Mar 06		G339.75-0.9	16 49 59.5	-46 01 02	1990 Jun 11
G291.0+0.0	11 11 58.9	-60 32 49	1992 Jun 05		G339.75+0.9	16 42 11.5	-44 50 51	1989 May 26
G291.375-0.9	11 12 04.4	-61 31 19	1991 Oct 05		G340.25+0.0	16 47 53.5	-45 03 20	1986 Jun 26
G291.375+0.9	11 17 25.9	-59 50 44	1989 Feb 21		G340.75-0.9	16 53 37.8	-45 14 44	1990 Jun 12
G291.4-0.6	11 13 38.7	-61 16 21	1994 Mar 03	N	G340.75+0.9	16 45 51.6	-44 05 30	1990 Jun 10
G291.6-0.5	11 15 09.6	-61 16 22	1991 Aug 16	N	G341.25+0.0	16 51 29.9	-44 17 17	1990 May 30
G291.75+0.0	11 17 41.2	-60 49 12	1993 Mar 08					1990 Jul 01
G292.125-0.9	11 17 57.5	-61 47 40	1992 Jun 28		G341.75-0.9	16 57 10.3	-44 28 02	1990 Jul 13
G292.125+0.9	11 23 03.5	-60 06 15	1989 Feb 24		G341.75+0.9	16 49 26.1	-43 19 42	1990 May 31
G292.38+0.0	11 22 28.8	-61 04 39	1990 Mar 10	N	G342.25+0.0	16 55 00.7	-43 30 50	1990 Jul 27
			1992 Mar 06	N	G342.75-0.9	17 00 37.3	-43 40 57	1989 Jun 01
G292.5+0.0	11 23 29.4	-61 04 40	1989 Feb 22		G342.75+0.9	16 52 55.1	-42 33 29	1990 Jul 20
G292.875-0.9	11 23 56.8	-62 03 05	1984 Mar 11		G343.1-0.6	17 00 36.2	-43 14 24	1990 Jun 13
G292.875+0.9	11 28 46.4	-60 20 51	1992 Apr 01		G343.25+0.0	16 58 26.1	-42 43 59	1990 Jul 10
G293.25+0.0	11 29 23.0	-61 19 11	1992 Mar 31		G343.75-0.9	17 03 58.9	-42 53 29	1989 Jun 02
G293.625-0.9	11 30 02.0	-62 17 30	1992 Mar 11		G343.75+0.9	16 56 18.9	-41 46 52	1989 May 31
G293.625+0.9	11 34 34.2	-60 34 31	1992 Jun 08		G344.25+0.0	17 01 46.4	-41 56 46	1990 Jul 11
G293.83-0.4	11 33 18.6	-61 46 35	1992 Mar 10	N	G344.4-0.3	17 03 32.1	-42 04 12	1991 May 17
G294.0+0.0	11 35 22.0	-61 32 44	1989 Mar 03		G344.75-0.9	17 07 15.6	-42 05 41	1989 Jun 04
G294.2-0.1	11 36 22.4	-61 42 44	1990 Mar 11	N	G344.75+0.9	16 59 37.8	-40 59 53	1989 May 30
G294.375-0.9	11 36 12.9	-62 30 55	1989 Mar 22		G345.25+0.0	17 05 01.8	-41 09 11	1992 Jun 01
G294.375+0.9	11 40 26.8	-60 47 13	1989 Mar 07		G345.4-0.9	17 09 34.4	-41 35 46	1994 Apr 21
G294.75+0.0	11 41 26.0	-61 45 17	1989 Mar 08		G345.75-0.9	17 10 27.3	-41 17 33	1990 Jul 12
G295.125-0.9	11 42 29.1	-62 43 19	1992 Mar 12		G345.75+0.9	17 02 51.9	-40 12 32	1992 May 07
G295.125+0.9	11 46 24.0	-60 58 56	1989 Mar 09		G346.0+0.5	17 05 28.6	-40 14 04	1991 May 21
G295.5+0.0	11 47 34.8	-61 56 49	1989 Mar 10		G346.25+0.0	17 08 12.6	-40 21 17	1993 May 13
G295.875-0.9	11 48 50.3	-62 54 39	1990 Mar 12		G346.75-0.9	17 13 34.5	-40 29 05	1993 Jun 02
G295.875+0.9	11 52 25.4	-61 09 38	1989 Mar 13		G346.75+0.9	17 06 01.5	-39 24 51	1991 May 22
G296.25+0.0	11 53 48.1	-62 07 18	1989 Mar 14		G347.25+0.0	17 11 18.8	-39 33 03	1990 Jul 15
G296.625-0.9	11 55 16.3	-63 04 55	1989 Mar 15		G347.75-0.9	17 16 37.3	-39 40 20	1992 Apr 30
G296.625+0.9	11 58 30.7	-61 19 19	1989 Mar 16		G347.75+0.9	17 09 06.7	-38 36 51	1991 Jun 07
G297.0+0.0	12 00 05.5	-62 16 44	1989 Mar 20		G348.25+0.0	17 14 20.8	-38 44 31	1992 Jul 21
G297.2+0.3	12 02 34.5	-61 59 43	1991 Jul 27	N	G348.75-0.9	17 19 35.9	-38 51 18	1992 May 13
G297.375-0.9	12 01 46.5	-63 14 05	1992 Mar 17		G348.75+0.9	17 12 07.8	-37 48 32	1991 Jun 10
G297.375+0.9	12 04 39.6	-61 27 58	1989 Mar 21		G349.25+0.0	17 17 18.6	-37 55 42	1990 Jul 16
G297.6-0.9	12 03 30.0	-63 14 43	1991 Jul 19	N	G349.75-0.9	17 22 30.5	-38 02 00	1991 May 27
G297.75+0.0	12 06 26.6	-62 25 06	1989 Mar 23		G349.75+0.9	17 15 04.8	-36 59 55	1992 May 12
G298.125-0.9	12 08 20.7	-63 22 08	1992 Mar 20		G349.9-2.3	17 28 56.6	-38 42 23	1994 Jul 05
G298.125+0.9	12 10 51.7	-61 35 33	1989 Apr 03		G350.25+0.0	17 20 12.6	-37 06 36	1991 May 12
G298.5-1.3	12 12 40.2	-62 52 41	1994 Mar 10	N				1992 Sep 13
G298.5+0.0	12 12 51.1	-62 32 21	1989 Apr 01		G350.3-0.7	17 23 24.2	-37 27 47	1991 May 28
G298.875-0.9	12 14 58.2	-63 29 03	1992 Jun 27		G350.4-0.8	17 23 54.3	-37 27 45	1991 May 29
G298.875+0.9	12 17 06.7	-61 42 04	1989 Apr 02		G350.75-0.9	17 25 21.3	-37 12 27	1991 Jun 17
G299.25+0.0	12 19 18.4	-62 38 31	1993 Mar 11		G350.75+0.9	17 17 58.1	-36 11 02	1991 May 23
G299.625-0.9	12 21 38.7	-63 34 49	1984 Mar 21					1993 May 18
G299.625+0.9	12 23 24.2	-61 47 30	1989 Apr 04		G351.25+0.0	17 23 02.9	-36 17 15	1991 Jun 16
G300.0+0.0	12 25 48.2	-62 43 33	1989 Apr 07		G351.4-0.4	17 25 22.4	-36 22 38	1991 Jun 21
			1993 Mar 12		G351.75-0.9	17 28 08.4	-36 22 39	1991 May 19
G300.375-0.9	12 28 21.6	-63 39 26	1989 Apr 09		G351.75+0.9	17 20 47.7	-35 21 53	1983 Jul 04
G300.375+0.9	12 29 43.6	-61 51 50	1989 Apr 08					1992 May 14
G300.5-0.3	12 29 50.0	-63 06 35	1991 Jul 05	N	G352.25+0.0	17 25 49.5	-35 27 39	1992 May 18
G300.75+0.0	12 32 20.0	-62 47 27	1984 Mar 22		G352.75-0.9	17 30 52.1	-35 32 38	1992 May 21
G300.87+0.9	12 33 56.4	-61 54 07	1983 Apr 14	N	G352.75+0.9	17 23 33.8	-34 32 29	1988 Jun 08
G301.125-0.9	12 35 06.5	-63 42 52	1988 Apr 06		G353.25+0.0	17 28 32.8	-34 37 49	1992 May 31
G301.125+0.9	12 36 04.6	-61 55 04	1988 Apr 05		G353.4-0.3	17 30 19.6	-34 42 17	1991 May 30
G301.5-1.0	12 38 15.4	-63 49 30	1991 Jun 14	N	G353.75-0.9	17 33 32.4	-34 42 24	1993 May 19
G301.5+0.0	12 38 53.2	-62 50 13	1992 Mar 18		G353.75+0.9	17 26 16.6	-33 42 51	1987 Jun 21
G301.875-0.9	12 41 52.7	-63 45 08	1990 Mar 13		G354.25+0.0	17 31 12.9	-33 47 46	1985 Jun 11
G301.875+0.9	12 42 26.8	-61 57 12	1993 Mar 16					1992 May 22
G302.1+0.9	12 44 26.9	-61 56 25	1990 Apr 01	N	G354.75-0.9	17 36 09.6	-33 51 57	1987 Jun 22
G302.25+0.0	12 45 27.4	-62 51 50	1983 Apr 05		G354.75+0.9	17 28 56.2	-32 52 59	1993 May 26
G302.625-0.9	12 48 39.6	-63 46 12	1985 Apr 09		G354.8-0.2	17 33 24.5	-33 23 21	1987 Jul 01
G302.625+0.9	12 48 49.6	-61 58 13	1986 Apr 08		G355.25+0.0	17 33 49.8	-32 57 30	1992 May 28
			1989 Apr 29		G355.75-0.9	17 38 43.8	-33 01 19	1991 Aug 09
G303.0+0.0	12 52 02.1	-62 52 18	1988 Apr 09		G355.75+0.9	17 31 32.8	-32 02 54	1987 Jun 28
G303.375-0.9	12 55 26.8	-63 46 06	1985 Apr 10		G356.25+0.0	17 36 23.8	-32 07 02	1985 Jun 13
G303.375+0.9	12 55 12.5	-61 58 07	1991 Apr 07					